PHYSICAL REVIEW B **90**, 121302(R) (2014)

Thermally enhanced photoinduced electron emission from nitrogen-doped diamond films on silicon substrates

Tianyin Sun, Franz A. M. Koeck, Aram Rezikyan, Michael M. J. Treacy, and Robert J. Nemanich*
Department of Physics, Arizona State University, Tempe, Arizona 85287-1504, USA
(Received 18 April 2014; revised manuscript received 20 August 2014; published 15 September 2014)

This work presents a spectroscopic study of the thermally enhanced photoinduced electron emission from nitrogen-doped diamond films prepared on *p*-type silicon substrates. It has been shown that photon-enhanced thermionic emission (PETE) can substantially enhance thermionic emission intensity from a *p*-type semiconductor. An *n*-type diamond/*p*-type silicon structure was illuminated with 400–450 nm light, and the spectra of the emitted electrons showed a work function less than 2 eV and nearly an order of magnitude increase in emission intensity as the temperature was increased from ambient to ∼400 °C. Thermionic emission was negligible in this temperature range. The results are modeled in terms of contributions from PETE and direct photoelectron emission, and the large increase is consistent with a PETE component. The results indicate possible application in combined solar/thermal energy conversion devices.

DOI: 10.1103/PhysRevB.90.121302 PACS number(s): 84.60.Jt, 79.40.+z, 79.60.Jv, 81.05.ug

Photons have been employed to generate electron emission from novel materials through various physical mechanisms [1,2]. Notably, a new emission mechanism that combines photoexcitation and thermal excitation, namely, photon-enhanced thermionic emission (PETE), has been proposed to describe results for Cs-coated *p*-type GaN [3]. Several theoretical studies have described possible applications of PETE in concentrated solar-thermionic energy conversion devices [4–11]. In a recent experimental study, photon-enhanced thermionic emission using a *p*-type GaAs/*p*-type AlGaAs heterojunction interface was explored [12], and the results indicated the spatial separation of photon absorption and electron emission in a PETE device. However, these prior results employed notably unstable cesiated surfaces to indicate the PETE effect. Studies involving new methods to decrease the emission barrier are therefore desirable.

Diamond films acquire a negative electron affinity (NEA) after hydrogen passivation [13–15] where the electron affinity is defined as the energy required to remove an electron from the conduction band minimum (CBM) of a semiconductor into vacuum away from the surface. For NEA diamond films, conduction band electrons can be readily emitted without overcoming an energy barrier. For crystalline diamond, *n*-type doping has been achieved by incorporation of nitrogen or phosphorus, with a donor level of nitrogen at 1.7 eV and that of phosphorus at 0.6 eV below the CBM [16,17]. The strong upward band bending often observed in *n*-type doped diamond can be mitigated in nanocrystalline diamond apparently because of the sp^2 bonds at the grain boundaries [18]. As a result, *n*-type doping of nanocrystalline diamond leads to lowering of the electron emission threshold, i.e., the effective work function Φ_W, which is defined for NEA materials to be the energy difference between the CBM and the Fermi level (E_F). Effective work functions of 1.3 eV with nitrogen doping and 0.9 eV with phosphorus doping have been reported for *n*-type chemical vapor deposited diamond [19,20]. These low work function surfaces enable visible light photoinduced electron emission and low temperature thermionic electron emission from diamond films on metallic substrates [21–23].

Based on these results, in this work we explore a two-layer configuration that combines a nitrogen-doped (*n*-type), hydrogen-terminated diamond film and a *p*-type semiconductor (i.e., silicon) substrate. The advantage of this structure is that the Si substrate is nearly ideal for absorption of the solar spectrum and the *p*-type character will enable a large increase of the electron quasi-Fermi level. The NEA *n*-type diamond film provides a low work function surface with potentially reduced recombination due to the lack of mobile holes.

A schematic of the emission mechanism is illustrated in Fig. 1: Photon-enhanced thermionic electrons are generated in the substrate, transported through the interface towards the diamond surface and contribute to the emission. Due to the wide band gap of diamond (∼5.5 eV at room temperature), it is presumed that the illuminating photons from the front side will be absorbed in the substrate. Alternatively, electrons can be generated directly from valence band states in the Si substrate and injected into the diamond layer without contributing to the enhanced population. This Rapid Communication presents an investigation of the photoinduced electron emission from nitrogen-doped (*n*-type) diamond films deposited on *p*-type Si substrates and its temperature dependence. The results are discussed in terms of the emission mechanisms.

The PETE model from the work by Schwede *et al.* [3] is based on a balance between photoexcitation and recombination in a single layer of material, which absorbs photons and emits electrons through the opposite surfaces. In a zero-dimensional simplification, the loss of electrons due to transport between the two surfaces is neglected, which provides a carrier distribution that is essentially identical to our front illumination experimental setup. In the following analysis [24], the fundamental relationships in both the PETE and the direct photoemission mechanisms are introduced, based on a single-layer film. To apply the two single-layer models to a diamond-Si bilayer structure, it is assumed that the emission threshold is determined by the interface conduction band barrier. Consequently the electron affinity χ is replaced with the value of this barrier as experimentally measured in the photoinduced emission spectra. Additionally, recombination due to the diamond-Si interface is also ignored, and ideal electron transport properties are assumed. These assumptions may be

*robert.nemanich@asu.edu

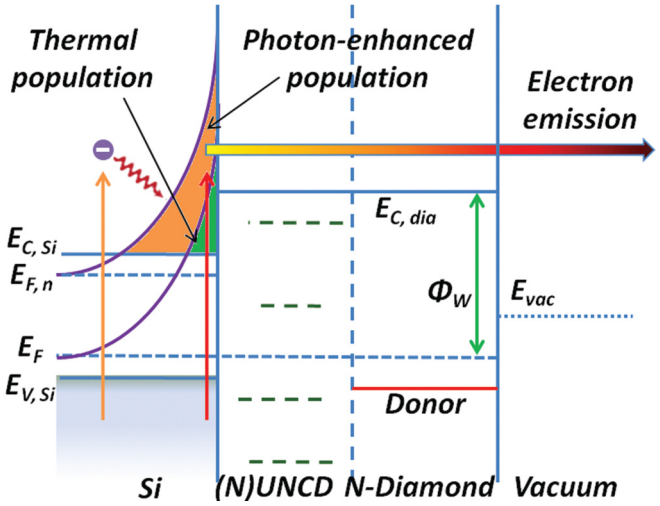

FIG. 1. (Color online) Band schematics of the proposed diamond-Si structure showing electrons being excited in the absorbing substrate and contributing to the photon-enhanced emission through the low work function surface.

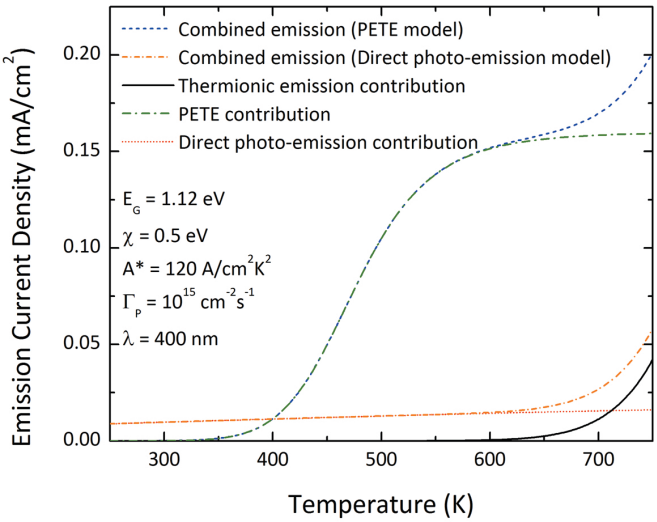

FIG. 2. (Color online) Simulation results of the two models on an ideal electron emitter, which has a band gap of 1.12 eV, electron affinity of 0.5 eV, and is under illumination of 400 nm light with a photon flux of 10^{15} cm^{-2} per second. The thermionic contribution is obtained by calculating the emission current with no photon illumination.

reasonable since recombination at Si interfaces is typically low and diffusion lengths of electrons in n-type diamond may be expected to be long due to the lack of free holes.

We first summarize the PETE model [3]. It is assumed that all photons with energy above the semiconductor band gap are absorbed and converted into conduction band electrons which follow a thermally stabilized Maxwell-Boltzmann distribution, and the enhanced emission current density is given in a form similar to the Richardson-Dushman relationship for "pure" thermionic electron emission:

$$J = A^* T^2 \exp\{-[\Phi_W - (E_{F,n} - E_F)]/k_B T\}$$
$$= e(n_{eq} + dn)\sqrt{\frac{k_B T}{2\pi m_n^*}}\exp[-\chi/k_B T], \quad (1)$$

where A^* is the Richardson constant of the emitter, T is the emitter temperature, $E_{F,n}$ is the electron quasi-Fermi level, k_B is the Boltzmann constant, m_n^* is the electron effective mass, n_{eq} is the equilibrium electron concentrations, dn is the enhanced electron population in the conduction band, and χ is the emission barrier height with respect to the CBM. Consequently, the PETE current intensity J can be found by solving dn and substituting into Eq. (1). We also note that a recent publication employed a modified PETE model that achieved good correspondence with experimental data [25].

It should be noted that recent considerations of the PETE model have focused mostly on p-type substrates. This is due to the fact that the enhancement in PETE is most significant when dn is significantly larger than n_{eq}, as shown in Eq. (1). For an n-type material, as electrons are the majority carriers, the relative enhancement from photon illumination will be considerably smaller compared to a p-type material under the same illumination conditions.

Direct photoelectron generation in a semiconductor, on the other hand, focuses on a nonequilibrium process, where the photoelectrons transport across the interface barrier before thermal relaxation. This calls for a separate analysis. This emission mechanism can be simulated by employing an internal photoemission model [26,27], which describes the quantum yield as a function of the energy of the illuminating photons:

$$Y(h\nu) = \frac{\int_0^{h\nu - E_G} T(E)S(E,h\nu)N_c(E)N_v(E - h\nu)dE}{\int_0^{h\nu - E_G} N_c(E)N_v(E - h\nu)dE}, \quad (2)$$

where N_c and N_v are the conduction band and valence band density of states (DOS) in the absorbing substrate. $T(E)$ and $S(E,h\nu)$ are the electron emission function and optical absorption function, respectively. The energy zero is the CBM. Assuming parabolic DOS for Si and diamond, the direct photogeneration spectrum using the specific diamond properties is obtained through a numerical calculation.

As an example, Fig. 2 shows the results of individually applying the two models to an ideal single-layer electron emitter based on p-type Si. The structure includes a constant emission threshold of 0.5 eV above the Si CBM (i.e., $\chi = 0.5$ eV), and is illuminated with 400 nm photons at a flux of 10^{15} cm^{-2} per second. We note that in both models the emission current is approximately proportional to the photon flux in the tested temperature range. Like other studies, the calculation uses the ideal Richardson constant of 120 A/cm^2 K^2. The results contain the net current density, and the components contributed by both the "pure" thermionic emission and the photoinduced emission mechanisms, respectively. A comparison between the two models shows different features: The direct photoemission is relatively constant within the tested temperature range, while the PETE-induced charge distribution is affected by temperature, and consequently the PETE model results in a more significant temperature dependence. For the specific barrier values employed here, the PETE model shows a much stronger increase of electron emission than the direct photoemission model. We note that under these conditions $E_{F,n}$ is positioned at ~0.78 eV above the valence band

maximum (VBM) at 300 K, and as the temperature is increased to 650 K it is reduced to ∼0.14 eV at 650 K due to increased recombination. At higher temperatures the thermal excitation of conduction band electrons become more significant than the photoinduced change of $E_{F,n}$.

In the experimental setup [24], the nitrogen-doped diamond films were deposited on boron-doped ([B]∼10^{19} cm^{-3}) single crystal Si(100) substrates by microwave plasma enhanced chemical vapor deposition. The combined photoinduced and thermionic electron emission spectra were recorded as a function of temperature, using a VSW HA50 hemispherical electron analyzer positioned normal to the sample surface and operated at ∼0.1 eV resolution. The electron emission spectra were referenced to the Fermi level (E_F) of the metallic sample holders which was calibrated with a gold foil. A −10 V bias was applied to the sample to overcome the analyzer work function and the spectra were corrected for the applied bias. The photon source was a focused Oriel 100W Xe arc lamp with associated bandpass filters to provide visible light photons, at an angle of ∼35° to the normal direction.

Figure 3 shows photoinduced components of the emission spectra collected while the sample was illuminated by selected wavelength photons. When measured at elevated temperatures, the sample also exhibited thermionic emission without photon illumination, which is shown in Fig. 3(d). The thermionic emission spectra (TE, "light-off") were subtracted from the combined emission ("light-on") to obtain the displayed photoinduced component. Note that the TE component was only significant at the highest temperature, where it was still substantially less than the photoinduced emission component. In contrast to the UV (21.2 eV) photoemission results, the visible light photoinduced emission spectra exhibited a higher threshold energy which decreased at elevated temperatures. At ∼400 °C where thermionic emission started to be significant, this threshold was found to be approximately the same as the surface work function (1.9 eV). This decrease in low energy cutoff is possibly due to an interface barrier that becomes less significant for transport at elevated temperatures.

Figure 4 shows the temperature dependence of the integrated spectral intensities for the various illuminating wavelengths. In this measurement series, the sample was illuminated with 400 to 450 nm (3.10 to 2.76 eV) photons at a flux of ∼10^{15} cm^{-2} per second, and the thermionic emission contribution was subtracted from the combined emission spectrum. At low temperatures, the intensity increases with increasing photon energy, as expected for photoemission.

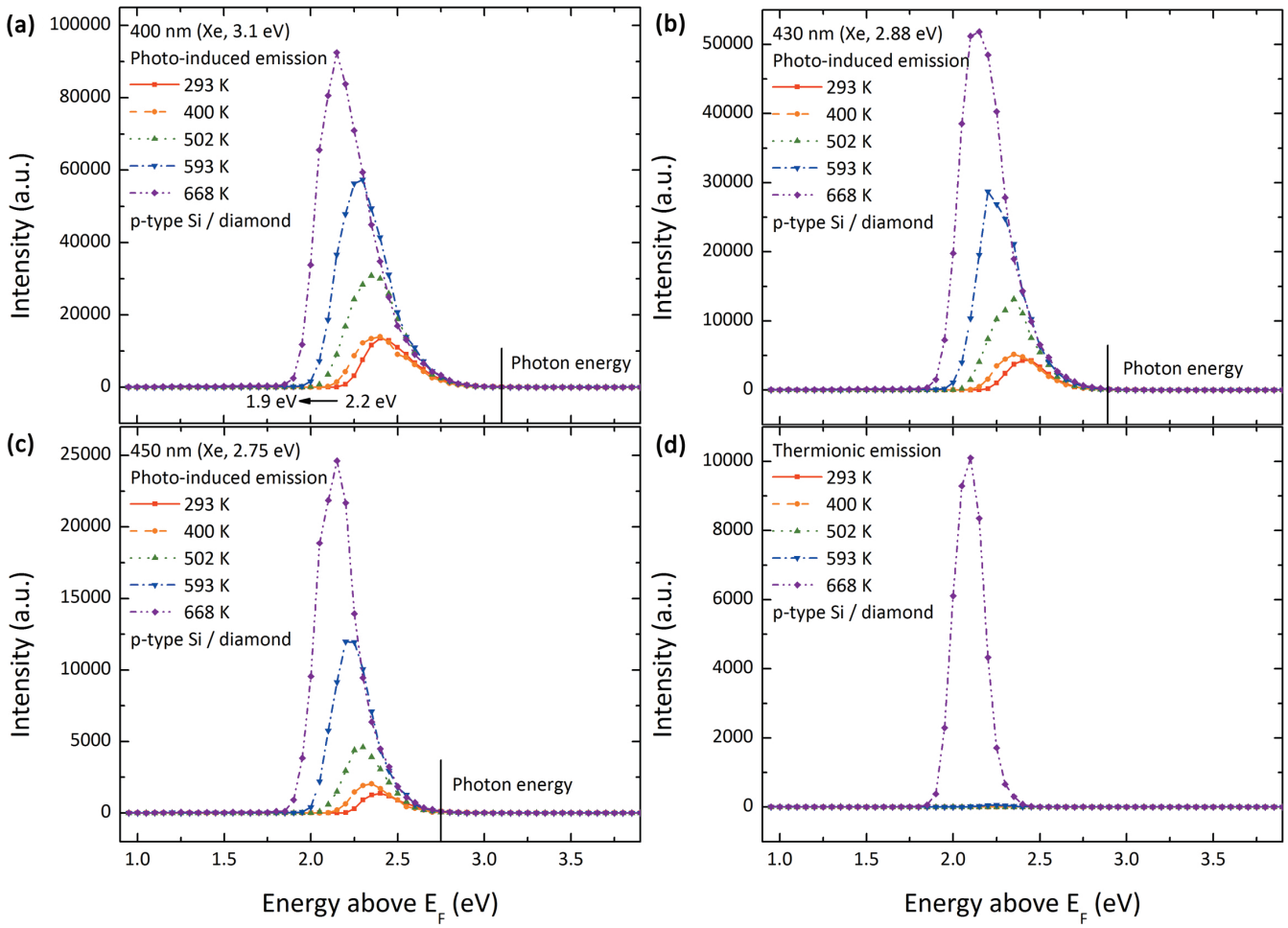

FIG. 3. (Color online) Photoinduced emission spectra from nitrogen-doped diamond films on a *p*-type doped Si substrate, obtained by subtracting the thermionic emission contribution from the combined emission spectra. The corresponding photon energies are labeled with solid lines relative to E_F. The "pure" thermionic emission spectra are shown in (d), and were collected at each temperature without illumination.

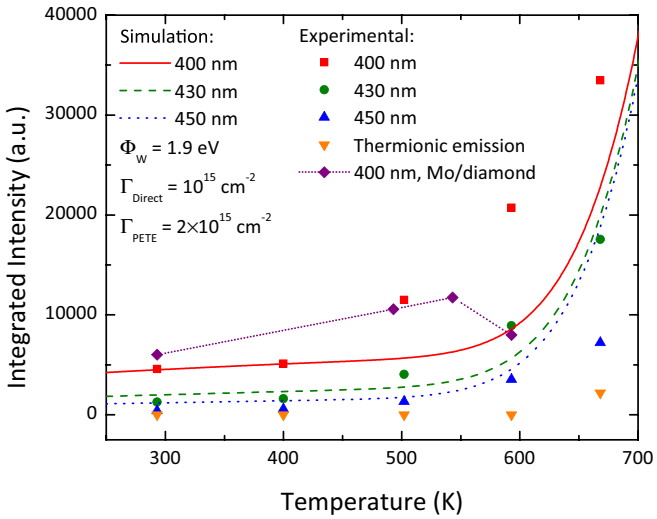

FIG. 4. (Color online) Temperature dependence of integrated photoinduced emission spectral intensity and thermionic emission intensity, obtained from a nitrogen-doped diamond film on a *p*-type doped Si substrate, showing results with different excitation energies. Results obtained from an N-doped diamond film on a Mo substrate [20] are also included for comparison. Combined curves of the two models are shown for the three wavelengths respectively.

As the sample temperature was increased to ~400 °C, the emission exhibited an intensity increase by a factor of ~7.3 to 18.4 for the different excitation energies. In contrast, this strong temperature dependence was not observed from diamond films deposited on metal substrates (also shown in Fig. 4). The diamond-metal samples have shown relatively constant photoinduced emission intensity [21,22], which is consistent with the conventional Fowler-DuBridge model [2,28] that only involves direct photoemission. These results are consistent with the model discussed here, since PETE is not expected from a metal substrate.

The modeling results of this N-doped diamond on *p*-type Si sample are represented by the curves in Fig. 4. The numerical calculations show the sum of emission intensities obtained from the two models, and are based on the temperatures and wavelengths used for the measurements. A photoemission barrier of 1.9 eV was employed in the simulations. The collection efficiency of the system was varied to fit the results obtained from the different methods. We found that with a photon flux ratio of 1:2 between the direct photoemission model and the PETE model, the simulation presented a temperature dependence that was similar to the experimental results.

The measurements were repeated for several samples prepared under different conditions. All samples showed similar results with variations in work function and enhancement factors. The samples were also found to show degradation after measurements at high temperature, and the photon enhancement was substantially reduced in repeated experiments. This could be related to changes of the interface properties and needs further study.

The key question of this study is whether PETE is observed. Most significantly, the diamond on Si showed a substantial increase in intensity as the temperature was increased, while for diamond on metals the intensity was approximately constant with temperature [21,22]. This comparison indicates that the PETE mechanism is consistent with the emission intensity increase for diamond films on Si substrates.

Meanwhile, there is also evidence that suggests the significance of emission mechanisms other than PETE. At lower temperatures (below 200 °C) photoinduced emission can be observed, although the PETE model predicts negligible emission under such conditions. Also, while showing significant temperature dependence, the photoinduced spectra of the diamond-Si samples still show similarities to the results collected from diamond films deposited on metal substrates. For instance, the spectral intensity shows a dependence on the photon energy, where the maximum electron kinetic energy in the spectrum approximately corresponds to the energy of the illuminating photons. Previously it was concluded that these high-energy electrons are from direct excitation of states near E_F [21]. For the PETE mechanism, however, the emission spectra are expected to be almost independent of photon energy [3], since the photoelectrons are thermally stabilized into a Maxwell-Boltzmann distribution regardless of the excitation energy. This supports the direct-generation model, as E_F in a heavily doped *p*-type Si wafer is close to the VBM. Therefore, direct generation of photoelectrons should be considered in the observed photoinduced electron emission.

The role of defects in both photogeneration and transport has not yet been considered in the models discussed above. Moreover, the actual generation and transport of photoelectrons can be a complex process. In our recent study of N-doped diamond on metal substrates [23], it was concluded that the photoelectrons may be generated in the substrate or in the nucleation layer which has a higher density of sp^2 bonds in the grain boundaries. The photon energy dependence shown in Fig. 4 may also be related to smaller optical absorption in the Si substrate for lower-energy photons, so that electrons generated deeper in the substrate may contribute less to the observed emission. These results indicate the complexity of the emission process that the two simplified models we examined cannot independently describe. A more advanced model would be necessary to better assess the specific mechanisms of the more complex double-layer structure.

The relative significance of the PETE and direct-generation processes may be related to the properties of the absorbing substrate material. The material will more likely exhibit PETE if forming a quasiequilibrium population of photoexcited electrons is more favorable than direct injection of the electrons across the barrier. Additionally, an optimal band gap of the substrate is required to absorb a wide solar spectrum, and it is necessary to limit surface and bulk recombination. We have assumed that a semiconductor with an indirect band gap (e.g., Si) will enable PETE-type emission, due to reduced cross-gap recombination and a longer electron relaxation time. These properties, and the NEA of diamond surfaces, lead to the proposed structure in this work. Theoretically, the optimal band gap for PETE materials has been predicted to be ~1.4 eV [3,6], and candidate substrates including GaAs and InGaN may be appropriate. To develop high efficiency PETE devices, it is important to understand the transport and recombination properties of these materials.

To conclude, a significant increase of photoinduced electron emission at elevated temperatures has been observed from

nitrogen-doped diamond films on *p*-type silicon substrates. The results differ from previously reported features of diamond emitters on metal substrates, where a relatively constant photoinduced emission was observed. The results are consistent with PETE, which involves generation of an enhanced electron population and lowering of the emission barrier due to the diamond film. Computer-based modeling is employed to compare different physical mechanisms, and the results appear to indicate a complex generation process. As significant enhancement of electron emission is shown through combined excitation from heat and light, such diamond emitters could potentially be applied in concentrated solar collection systems for solar-thermionic energy conversion. Examination of different substrate candidates to optimize the PETE contribution will be important in the future.

We gratefully acknowledge the LeRoy Eyring Center for Solid State Science at Arizona State University for the use of the aberration corrected microscope. This work is supported through the Office of Naval Research under Grant No. N00014-10-1-0540.

[1] M.V. Moghaddam, P. Yaghoobi, and A. Nojeh, Appl. Phys. Lett. **101**, 253110 (2012).
[2] P. T. McCarthy, S. J. Vander Laan, D. B. Janes, and T. S. Fisher, J. Appl. Phys. **113**, 193710 (2013).
[3] J. W. Schwede, I. Bargatin, D. C. Riley, B. E. Hardin, S. J. Rosenthal, Y. Sun, F. Schmitt, P. Pianetta, R. T. Howe, Z. X. Shen, and N. A. Melosh, Nat. Mater. **9**, 762 (2010).
[4] A. Varpula and M. Prunnila, J. Appl. Phys. **112**, 044506 (2012).
[5] T. Ito and M. A. Cappelli, Appl. Phys. Lett. **101**, 213901 (2012).
[6] K. Sahasrabuddhe, J. W. Schwede, I. Bargatin, J. Jean, R. T. Howe, Z.-X. Shen, and N. A. Melosh, J. Appl. Phys. **112**, 094907 (2012).
[7] G. Segev, A. Kribus, and Y. Rosenwaks, Sol. Energy Mater. Sol. Cells **113**, 114 (2013).
[8] G. Segev, Y. Rosenwaks, and A. Kribus, J. Appl. Phys. **114**, 044505 (2013).
[9] S. Su, H. Zhang, X. Chen, J. Kang, and J. Chen, Sol. Energy Mater. Sol. Cells **117**, 219 (2013).
[10] Y. Yang, W. Yang, W. Tang, and C. Sun, Appl. Phys. Lett. **103**, 083902 (2013).
[11] S. Su, Y. Wang, T. Liu, G. Su, and J. Chen, Sol. Energy Mater. Sol. Cells **121**, 137 (2014).
[12] J. W. Schwede, T. Sarmiento, V. K. Narasimhan, S. J. Rosenthal, D. C. Riley, F. Schmitt, I. Bargatin, K. Sahasrabuddhe, R. T. Howe, J. S. Harris, N. A. Melosh, and Z.-X. Shen, Nat. Commun. **4**, 1576 (2013).
[13] F. J. Himpsel, J. A. Knapp, J. A. VanVechten, and D. E. Eastman, Phys. Rev. B **20**, 624 (1979).
[14] B. B. Pate, Surf. Sci. **165**, 83 (1986).
[15] J. van der Weide, Z. Zhang, P. K. Baumann, M. G. Wensell, J. Bernholc, and R. J. Nemanich, Phys. Rev. B **50**, 5803 (1994).
[16] R. G. Farrer, Solid State Commun. **7**, 685 (1969).
[17] K. Haenen, K. Meykens, M. Nesladek, G. Knuyt, L. M. Stals, T. Teraji, S. Koizumi, and E. Gheeraert, Diamond Relat. Mater. **10**, 439 (2001).
[18] S. Bhattacharyya, Phys. Rev. B **70**, 125412 (2004).
[19] F. A. M. Koeck and R. J. Nemanich, Diamond Relat. Mater. **18**, 232 (2009).
[20] F. A. M. Koeck, R. J. Nemanich, A. Lazea, and K. Haenen, Diamond Relat. Mater. **18**, 789 (2009).
[21] T. Sun, F. A. M. Koeck, C. Zhu, and R. J. Nemanich, Appl. Phys. Lett. **99**, 202101 (2011).
[22] N. Neugebohrn, T. Sun, F. A. M. Koeck, G. G. Hembree, R. J. Nemanich, T. Schmidt, and J. Falta, Diamond Relat. Mater. **40**, 12 (2013).
[23] T. Sun, F. A. M. Koeck, P. B. Stepanov, and R. J. Nemanich, Diamond Relat. Mater. **44**, 123 (2014).
[24] See Supplemental Material at http://link.aps.org/supplemental/10.1103/PhysRevB.90.121302 for experimental and modeling details.
[25] W. Tang, W. Yang, Y. Yang, C. Sun, Z. Cai, Mater. Sci. Semicon. Process. **25**, 143 (2014).
[26] N. B. Kindig and W. E. Spicer, Phys. Rev. **138**, A561 (1965).
[27] R. J. Powell, J. Appl. Phys. **41**, 2424 (1970).
[28] R. H. Fowler, Phys. Rev. **38**, 45 (1931).